Disentangling the Inviscid and Viscous Energy Saving Mechanisms of Intermittent Swimming

Emre Akoz,[*] Geng Liu,[†] Pan Han,[‡] Haibo Dong,[§] and Keith W. Moored[¶]

Numerous studies have examined unsteady bio-inspired propulsion by assuming that aquatic animals oscillate their fins with continuous, sinusoidal motions. However, there are many fish such as saithe, cod and zebra danios that use a non-continuous or intermittent swimming gait. This burst-and-coast behavior has be shown to save as much as 50% of the energy it takes to swim a given distance for some kinematic motions and was originally hypothesized to be due to a viscous mechanism known as the Bone-Lighthill boundary layer thinning hypothesis. Recently, it has been shown that there is also an inviscid Garrick mechanism that can account for most of the observed energy savings. Here, our goal is to determine the relative contributions from the inviscid and viscous mechanisms to the total energy savings. To accomplish this we compare the performance and flow structures of a self-propelled pitching hydrofoil from an inviscid boundary element method (BEM) with those from direct numerical simulations (DNS). The DNS solutions range from $Re \approx 3000 - 6000$ and exhibit significantly more complex boundary layer and wake flows, however, many of the large-scale structures are captured in the BEM solutions. One DNS flow feature that is not captured in the BEM solutions is the formation and shedding of additional leading-edge vortices during the bursting and coasting phases of motion. These vortices lead to additional form drag during coasting that is not present in the inviscid simulations. For the Reynolds number range of the simulations, the maximum energy savings calculated by DNS are 17% and 20% for $\theta_0 = 15°$ and $\theta_0 = 20°$, respectively. For comparable BEM simulations the maximum energy savings are 14% and 24% for $\theta_0 = 15°$ and $\theta_0 = 20°$, respectively, showing good agreement between both numerical methods. Finally, it is shown that for low Re on the order of $\mathcal{O}(10^3)$ the inviscid Garrick mechanism is shown to account for nearly the entire energy savings of intermittent swimming, while in the high Re limit it is estimated that half of the energy savings comes from the inviscid mechanism and the other half comes from the viscous Bone-Lighthill mechanism.

Nomenclature

ρ	density of the fluid
f	frequency
θ_0	maximum pitching angle
A	tip-to-tip amplitude
S_p	planform area of the propulsor
M	mass of the hydrofoil
DC	duty cycle
t	time
$\overline{T}$	Time-averaged thrust
$\overline{P}$	Time-averaged power

[*]PhD Student, Department of Mechanical Engineering and Mechanics, Lehigh University, Bethlehem, PA, 18015, USA.

[†]Postdoctoral Research Associate, Department of Mechanical and Aerospace Engineering, University of Virginia, Charlottesville, VA, 22904, USA.

[‡]PhD Student, Department of Mechanical and Aerospace Engineering, University of Virginia, Charlottesville, VA, 22904, USA.

[§]Associate Professor, Department of Mechanical and Aerospace Engineering, University of Virginia, Charlottesville, VA, 22904, USA.

[¶]Assistant Professor, Department of Mechanical Engineering and Mechanics, Lehigh University, Bethlehem, PA, 18015, USA.

American Institute of Aeronautics and Astronautics

D Drag
U swimming speed
$\overline{U}$ Time-averaged swimming speed
S_w Wetted area
Re Reynolds number
C_T Coefficient of thrust
CoT Cost of transport
$\hat{CoT}$ Normalized cost of transport

I. Introduction

Aquatic animals use a variety of locomotion mechanisms and swimming gaits to propel themselves fast and efficiently through the oceans.[1] Some caudal fin swimmers such as saithe,[2] cod[3] and zebra danios[4] use an intermittent swimming gait known as burst-and-coast or burst-and-glide swimming. It was first hypothesized[5] and then later verified[4,6,7] that interspersing a coasting phase between steady swimming cycles can save on the order of 50% of the energy for some fish to swim a given distance.[7]

Classically, the observed energy savings has been attributed to the Bone-Lighthill boundary layer thinning hypothesis.[6] This mechanism supposes that the skin friction drag coefficient is higher during the bursting phase of swimming and lower during the coasting phase due to the thinning of the boundary layers on a fish body when undulating.[5,8,9] This has been observed in biology by Anderson et $al.$[10] where they measured a skin friction drag rise of 50–90% for swimming scup and dogfish as compared to still fish in a Reynolds number range of $Re = \mathcal{O}(10^3)$–$\mathcal{O}(10^5)$. On the contrary, Yanase & Saarenrinne[11,12] reported PIV measurements on a swimming trout where they concluded that although the skin friction increases on one side of the fish the opposite side of the fish has a skin friction decrease canceling out the net skin friction rise when averaged over the full cycle of motion. However, Ehrenstein et al.[8,9] conducted detailed numerical studies on both two- and three-dimensional oscillating and static plates at $Re = 200$ reporting a 20% increase in the skin friction drag of two-dimensional plates and a 70–100% increase in the skin friction drag of three-dimensional plates, respectively. These numerical studies conclusively showed that a skin friction rise can occur due to boundary layer thinning on oscillating bodies. Yet, what is unclear is whether the observed energy savings for intermittent swimmers can be fully attributed to this viscous mechanism.

In fact, recently an energy savings as high as 68% is observed in computations conducted on $inviscid$ intermittently swimming two-dimensional pitching hydrofoils,[13] which is on the same order as the energy savings observed in previous studies.[6,7,14,15] For these computations there was no boundary layer model being used, but instead a U^2 drag law with a $fixed$ drag coefficient is prescribed that importantly does not change during the bursting or coasting phases. The observed inviscid energy savings was attributed to a Garrick mechanism where by varying the duty cycle of motion there is an increase in the ratio of the added-mass thrust producing forces compared to the circulatory drag-inducing forces, which improves the efficiency of locomotion. This newly discovered inviscid mechanism now gives a framework to better understand the energy savings of intermittent swimming.

It is expected that both the inviscid and viscous mechanisms contribute to the energy savings observed in real flows, however, the importance of each effect is unclear. Therefore the aim of this study is to (1) fully resolve the benefit coming from intermittent swimming in a viscous fluid and to (2) determine how much of the benefit is coming from the skin friction/form drag rise during bursting and how much of it is associated with the alteration of the ratio of added-mass thrust to circulatory drag-inducing forces.

II. Approach and Methods

An inviscid as well as a viscous model are employed to differentiate the viscous and inviscid mechanisms contributing to the burst and coast swimming benefit.

A. Boundary Element Method

An unsteady potential flow method is employed to calculate the flow field around the free swimming hydrofoils. We defined the free swimming problem in an inertial reference frame which is fixed to the undisturbed

American Institute of Aeronautics and Astronautics

fluid. The velocity, $\mathbf{u}$, can be defined as; $\mathbf{u} = \nabla\phi^*$, where ϕ^* is the perturbation potential defined in the inertial frame. Then, in an incompressible, irrotational fluid flow, continuity equation is reduced to Laplace's equation, $\nabla^2\phi^* = 0$. Laplace's equation is solved subject to two boundary conditions; (1) no flux boundary condition, i.e. no flux through the body boundaries, and (2) far field boundary condition, i.e. the flow disturbances caused by the body must decay far away. Following Katz & Plotkin, Quinn et. al. and Akoz & Moored,[13, 16, 17] the general solution for the Laplace's equation is reduced to finding a distribution of doublets and sources on the hydrofoil surface and in the wake that satisfy the no-flux boundary condition on the body at each time step. Doublets and sources both implicitly satisfy the far-field boundary condition. We use the Dirichlet formulation to satisfy the no-flux condition on the foil body.

To solve this problem numerically, the hydrofoil is discretized into constant-strength source and doublet boundary elements and wake is discretized into doublet elements. Enforcing no flux boundary condition by assigning a collocation point for each boundary element on the hydrofoil leads to a linear system of equations. The system of equations are underdetermined with N equations and $N + 1$ unknowns. An explicit Kutta condition is applied to force the vortex shedding from the trailing edge by setting the trailing edge velocity to zero. Setting the trailing edge velocity results in a determinate system of linear equations which can be solved for the body doublet strengths. Once the perturbation potential is solved, the perturbation velocity on the body is determined by a local differentiation of the perturbation potential. Then, the pressure field acting on the body is calculated by using the unsteady Bernoulli equation. Then, the forces acting on the pitching airfoil is calculated by integration of the pressure forces over the hydrofoil boundary.

At every time step, one wake panel is shed from the hydrofoil whose doublet strength is dictated by the explicit Kutta condition and its strength remains fixed for all time. Shed panels advects with the local induced velocity field from the other wake and body elements. During this rollup process, the endpoints of the doublet elements, which are mathematically equivalent to point vortices, must be desingularized for the numerical stability of the solution. Following Krasny,[18] the induced velocity on a wake element from other doublet elements is then calculated with a desingularized Biot-Savart law.

B. Immersed Boundary Method

The pitching foil is treated as an immersed moving boundary in our in-house immersed-boundary-method-based computational fluid dynamics (CFD) solver. The numerical methodology employed in the current study is briefly introduced as the following. The 2D incompressible Navier-Stokes equations were discretized using a cell-centered, collocated arrangement of the primitive variables, and was solved using a finite difference-based Cartesian grid immersed boundary method.[19] The immersed-boundary treatment is the same as that in.[20] The equations were integrated in time using the fractional step method, which consists of three-steps. In the first sub-step of this method, a modified momentum equation is solved. A second-order, Adams-Bashforth scheme is employed for the convective terms while the diffusion terms are discretized using an implicit Crank Nicolson scheme which eliminates the viscous stability constraint. A second-order central difference scheme is employed in space discretization. This method was successfully applied in many simulations of flapping propulsion.[21–24] More details about this method can be found in Mittal et al. and Dong et al.[19, 20] Validations about this solver can be found in our previous work o fWan et. al. and Li et al.[23, 25]

C. Problem Formulation

To fully resolve the intermittent swimming benefit and separate the viscous and inviscid mechanisms contributing to the benefit, an inviscid as well as a DNS study is performed with two-dimensional self-propelled hydrofoils. In the inviscid computations, an empirical drag law is employed to account for the skin friction and form drag experienced by the hydrofoils. Skin friction drag coefficients are acquired from continuously swimming and static hydrofoils for a range of Reynolds numbers (Re) in steady swimming conditions from the DNS solutions (see Figure 1a-b). Then, a second order polynomial fit is applied to estimate the skin friction drag coefficient based on the Reynolds number of the swimmer. Figure 1c shows the skin friction coefficient as a function of Re number for static and swimming hydrofoils and the shaded gray region represents the Reynolds number range of the current study. On the other hand, Figure 1d shows the skin friction coefficient change of a hydrofoil from static to swimming states as a function of Reynolds number and Δ is defined as,

American Institute of Aeronautics and Astronautics
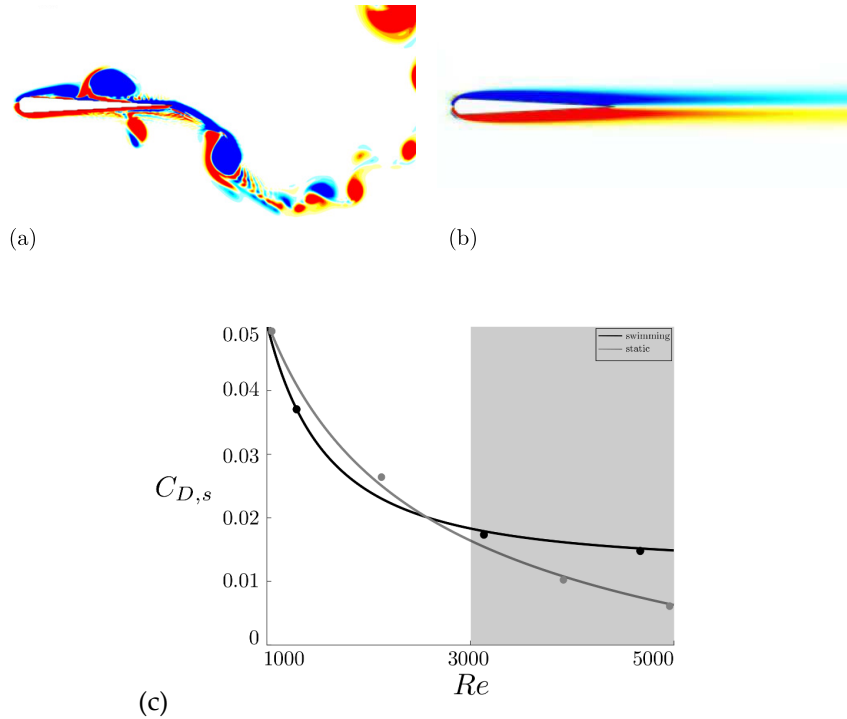
(a)   (b)

(c)

Figure 1: (a) Vorticity field of a swimming airfoil. (b) Vorticity field of a static airfoil. (c) Skin friction coefficient of a swimming and a static airfoil as a function of Reynolds number. Shaded areas in (c) represent the Reynolds number range of the current study.

$$\Delta = \frac{C_{D,s}^{swim} - C_{D,s}^{static}}{C_{D,s}^{static}} \tag{1}$$

where $C_{D,s}^{swim}$ and $C_{D,s}^{static}$ are the skin friction coefficients of the swimming and static hydrofoils, respectively. The skin friction of a static hydrofoil rises 30-136% once it starts to swim within the Re number range of $3.2 \times 10^3 - 5 \times 10^3$. This observation is in line with the recent reported results.[8–10] However, an enhancement of 3-10 folds as predicted by previous studies[3, 5, 15, 26], seems unlikely.

The total drag coefficient is assumed to be a linear combination of the skin friction drag ($C_{D,s}$) and the form drag coefficients ($C_{D,f}$). Form drag coefficient is chosen to be a constant value which ensures that the average cruising velocity of the inviscid and viscous simulations are in the same range.

To distinguish the energy savings coming from viscous and inviscid mechanisms, three set of simulations are studied with the BEM solver. The drag coefficient is varied among these three set of simulations to understand the effect of (1) inviscid mechanism, (2) skin friction change in between bursting and coasting phases and (3) form drag change in between bursting and coasting phases contributions to the intermittent gait energy savings. Drag forces associated to the three cases of simulations can be summarized as follows;

American Institute of Aeronautics and Astronautics

$$\text{case 1} \quad D = \begin{cases} (C_{D,s}^{swim} + C_{D,f}^{swim})\rho S_p U^2, & 0 \leq t \leq T_{\text{burst}} \\ (C_{D,s}^{swim} + C_{D,f}^{swim})\rho S_p U^2, & T_{\text{burst}} \leq t \leq T_{\text{cycle}} \end{cases} \tag{2}$$

$$\tag{3}$$

$$\text{case 2} \quad D = \begin{cases} (C_{D,s}^{swim} + C_{D,f}^{swim})\rho S_p U^2, & 0 \leq t \leq T_{\text{burst}} \\ (C_{D,s}^{static} + C_{D,f}^{swim})\rho S_p U^2, & T_{\text{burst}} \leq t \leq T_{\text{cycle}} \end{cases} \tag{4}$$

$$\tag{5}$$

$$\text{case 3} \quad D = \begin{cases} (C_{D,s}^{swim} + C_{D,f}^{swim})\rho S_p U^2, & 0 \leq t \leq T_{\text{burst}} \\ (C_{D,s}^{static} + C_{D,f}^{static})\rho S_p U^2, & T_{\text{burst}} \leq t \leq T_{\text{cycle}} \end{cases} \tag{6}$$

where C_{form}^{swim} and C_{form}^{static} are the form drag coefficients of the swimming and static hydrofoils, respectively. ρ is the density of the fluid, S_p is the propulsor surface area and U is the speed of the swimmer. T_{burst} is the bursting period of the cycle and T_{cycle} is the total cycle period.
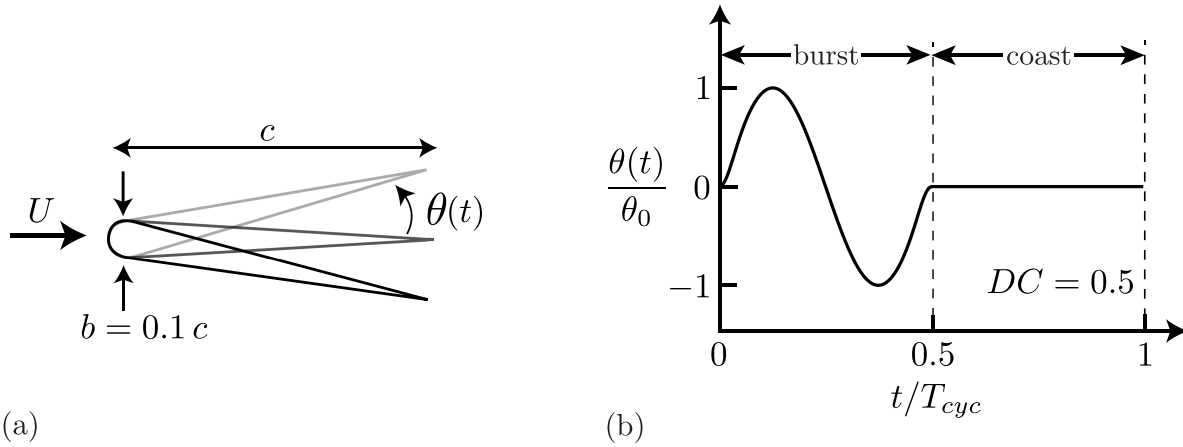

Figure 2: (a) Geometric and numerical parameters for the teardrop hydrofoil. (b) Normalized pitching angle as a function of normalized time for an intermittent swimmer with DC = 0.5.

A teardrop airfoil is chosen for the current study as shown in Figure 2a which has a semicircular leading edge and tapers along straight lines to its trailing edge. The maximum thickness of the airfoil is set to be 10% of its chord length. The chord and span lengths of the airfoil are $c = 0.05$m and $s = 0.05$m, respectively. The ratio of bursting to costing is controlled by the duty cycle parameter,

$$DC = \frac{\text{burst period}}{\text{total cycle period}} \tag{7}$$

Hydrofoils are pitched with respect to their leading edges. The intermittent motion is a combination of a sinusoidal pitching motion for the burst period and it is followed by a fixed pitch angle of $\theta = 0$ for the duration of the coast period. The total cycle period is simply the addition of the burst and coast periods. The combined burst and coast pitching motions about the leading edge of the hydrofoil is then defined as,

$$\theta(t) = \begin{cases} y_s(t)\left[\theta_0 \sin\left(2\pi f t\right)\right], & 0 \leq t \leq T_{\text{burst}} \\ 0, & T_{\text{burst}} \leq t \leq T_{\text{cycle}} \end{cases} \tag{8}$$

$$\text{where} \quad y_s(t) = \begin{cases} -\tanh(m\,t)\tanh\left[m\left(t-1\right)\right], & DC < 1 \\ 1, & DC = 1 \end{cases} \tag{9}$$

where θ_0 is the maximum pitch angle, f is the oscillation frequency and t is the time (See Figure 2b). Equation (8) defines a reference signal where $0 \leq t \leq T_{\text{cycle}}$. The signal used in the simulations has N_{cyc}

American Institute of Aeronautics and Astronautics

repetitions of this reference signal. Here, $T_{\text{burst}} = 1/f$ and $T_{\text{cycle}} = T_{\text{burst}}/DC$. Two maximum pitch angles are used in the current study, $\theta_0 = 15°$ and $\theta_0 = 20°$.

In order to obtain discretization independent solutions as the time step size is reduced, the discontinuous angular rates and accelerations at the junction of the burst phase and coast phase must be smoothed. To do this, a hyperbolic tangent envelope function, $y_s(t)$, is multiplied with the sinusoidal burst signal and is defined in (9). This function modifies the slope of the sine wave at $t/T_{\text{burst}} = 0$ and $t/T_{\text{burst}} = 1$ to ensure a desingularized smooth junction with the coast phase where m controls the radius of curvature of the junction. In the current study, $m = 30$ is used. Additionally, if $DC = 1$, then the signal (8) reverts to a continuous sinusoidal signal. In the current study the duty cycle ranges from $DC = 0.2$ to $DC = 1$ in 0.1 increments. A summary of the input parameters used in the current study are in Table 1.

Continuous Swimmers								
f (Hz)	0.25	0.5	0.75	1				
DC	1							
θ_0 (deg.)	15	20						

Intermittent Swimmers								
f (Hz)	1							
DC	0.2	0.3	0.4	0.5	0.6	0.7	0.8	0.9
θ_0 (deg.)	15	20						

Table 1: Simulations parameters used in the present study.

The mean cruising velocity, $\overline{U}$, mean thrust, $\overline{T}$, and mean power $\overline{P}$, are calculated once the swimmers have reached their steady state swimming conditions. The mean thrust force is calculated as the streamwise force from the integration of the pressure forces only. The mean power input to the fluid is calculated as the negative inner product of the force vector and velocity vector of each boundary element. Cost of transport (CoT), which is defined as the amount of energy it takes to travel a unit distance per unit mass, is another important performance parameter used in the current study. The thrust coefficient and cost of transport are defined as,

$$C_T \equiv \frac{\overline{T}}{\rho S_p f^2 A^2} \qquad\qquad CoT \equiv \frac{\overline{P}}{m\overline{U}} \qquad\qquad (10)$$

The ratio of CoT values of intermittent to continuous swimmers at the same mean speed will give the energy savings observed by choosing either mode of swimming. The ratio can be defined as,

$$\hat{CoT} = \frac{CoT^i|_{\overline{U}}}{CoT^c|_{\overline{U}}} \qquad\qquad (11)$$

where CoT^i and CoT^c are the cost of transports for the intermittent and continuous swimmer, respectively.

III.   Results

A.   Wake Dynamics and Thrust Profiles

Figure 3a-d shows the vorticity field of intermittent swimmers operating at $DC = 0.2$ in a viscous flow at slightly higher than $Re = 3000$. Four distinct vortices are shed from the trailing edge of the hydrofoil through the pitching motion. Vortex A and vortex D are shed as hydrofoil starts/stops pitching, respectively. Vortices B and C are shed as hydrofoil changes direction. Additionally, A-D vortex group perturbs the flow on the hydrofoil in the coasting period which in turn leads to shedding of extra vortices marked as E (See Figure 3c-d). The more hydrofoil coasts, the less extra vortices shed in the coasting phase and eventually
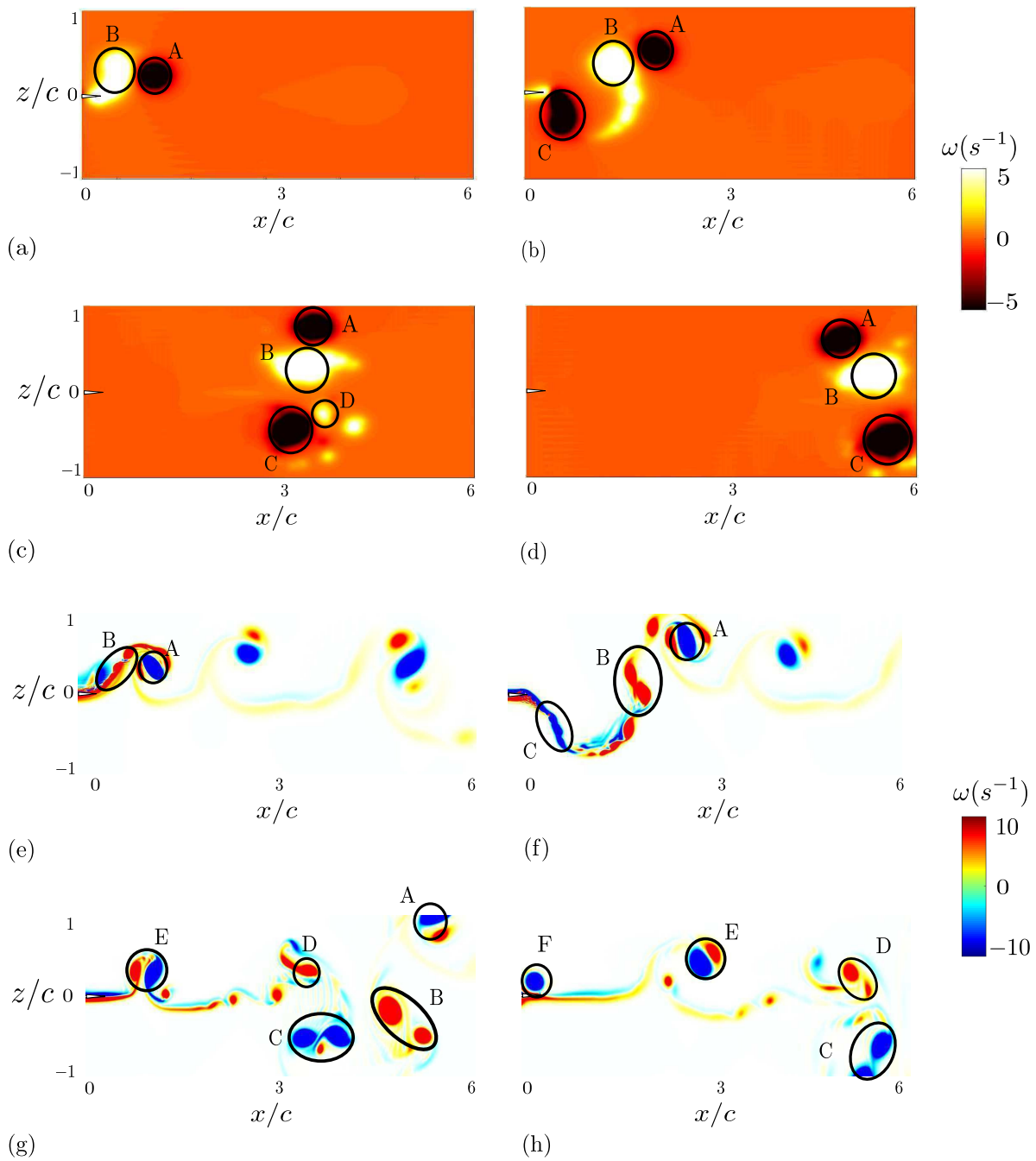
American Institute of Aeronautics and Astronautics

Figure 3: The evolution of the vortex wake is shown at times for a $DC = 0.2$ hydrofoil, (a),(e) $t/T_{cyc} = 1/10$, (b),(f) $t/T_{cyc} = 2/10$, (c),(g) $t/T_{cyc} = 4/10$, and (d),(h) $t/T_{cyc} = 6/10$ in viscous and inviscid flows, respectively.

flow field would converge to the static hydrofoil flowfield (See Figure 1b). Also, the higher the Re of the flow, the faster the flowfield converge to the static hydrofoil flowfield.

Similarly, Figure 3e-h shows the vorticity field of intermittent swimmers operating at $DC = 0.2$ in an inviscid flow. Four vortices are shed in the same manner as in the viscous case. However, in the coasting period extra vortices are not formed and the next bursting period starts to a less disturbed wake.
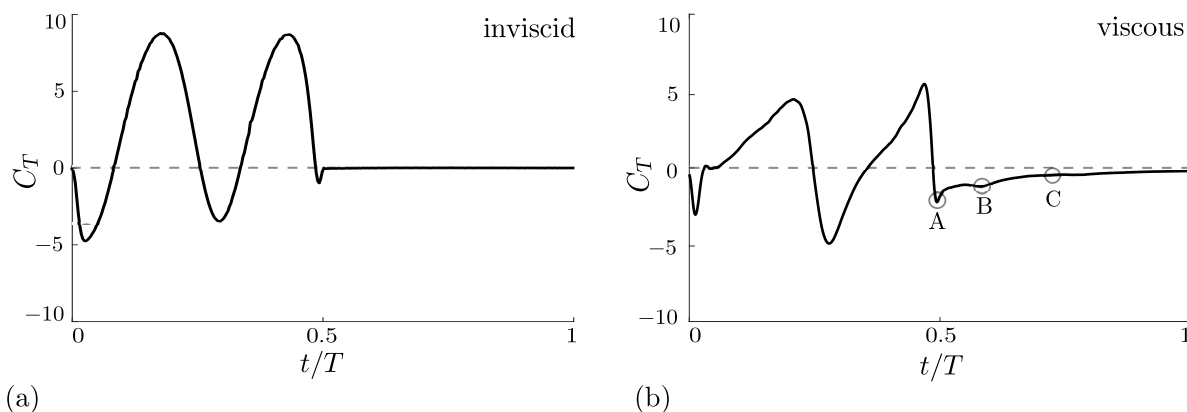

Figure 4: Thrust coefficients over a total period of an intermittent swimmer at $DC = 0.5$ in (a) an inviscid flow (b) a viscous flow.

Figure 4a-b shows the thrust generation of an intermittent swimmer at $DC = 0.5$ over a cycle as a function of time in inviscid and viscous flows, respectively. Swimmers show two peaks in thrust that are associated with the shedding of the two strongest vortices. Additionally, starting and stopping vortices create two dips in the thrust curves marked as A and B. The starting vortex induces a larger drag in the inviscid environment. On the other hand, the effect of stopping vortex on thrust is less pronounced in inviscid flow compared to the viscous flow. The hydrofoil swimming in the inviscid environment does not generate any thurst or experience any drag in the coasting period. However, hydrofoil operating in the viscous environment experiences drag in the coasting phase which is directly linked to the extra vortices shed in the coasting phase. As described previously, the influence of the extra vortices fade away further in the coasting period and thrust curve converges to zero.

B.   Performance and Energetics

Figure 5a-b and 5c-d show the cost of transport as a function of Re for maximum pitch angles of $\theta_0 = 15°$ and $\theta_0 = 20°$, respectively. The black markers represent continuous gait and white markers represent intermittent gait. Circles and squares are the results acquired in viscous and inviscid flows, respectively. Frequency of the continuous swimmers is varied in a range of $0.25 - 1$ Hz and as frequency of pitching increases so the Re and CoT. The intermittent swimmers have a fixed frequency of $f = 1$ Hz. At $DC = 1$ and $f = 1$ Hz, the intermittent and continuous swimmers are equivalent. When the duty cycle is decreased, the Re of the intermittent swimmer drops and consequently the CoT decreases.

Viscous simulations are plotted against inviscid simulations of drag law case 2 in Figure 5a-b, where skin friction decreases in the coasting phase as a function of the Re. It can be seen that for a range of Re and duty cycles, intermittent gait is more economical than the continuous one. Benefit of switching from continuous to intermittent gait increases with pitching amplitude and Re. The maximum energy savings are observed to be 17% and 20% in viscous flow for $\theta_0 = 15°$ and $\theta_0 = 20°$, respectively. In inviscid flow, on the other hand, maximum energy savings are 14% and 24% for $\theta_0 = 15°$ and $\theta_0 = 20°$, respectively.

Similarly, in Figure 5c-d viscous simulations are compared against inviscid simulations of drag law case 3, where coasting phase is modeled as a static hydrofoil. The response of CoT to changing pitching amplitude and Re is unchanged. However, absence of the extra vortices shed in the coasting phase in the case 3 model results in higher energy savings. The maximum energy savings from the inviscid simulations are 23% and 44% for $\theta_0 = 15°$ and $\theta_0 = 20°$, respectively. The benefits observed in the order of case 3 drag law could only be observed in high Re flows where coasting phase can be modeled as a static airfoil.

Figure 6 show the normalized cost of transport as a function of Re for three cases of drag laws studied for maximum pitch angles of $\theta_0 = 15°$ and $\theta_0 = 20°$, respectively. If $\hat{CoT} > 1$ then a continuous swimming gait
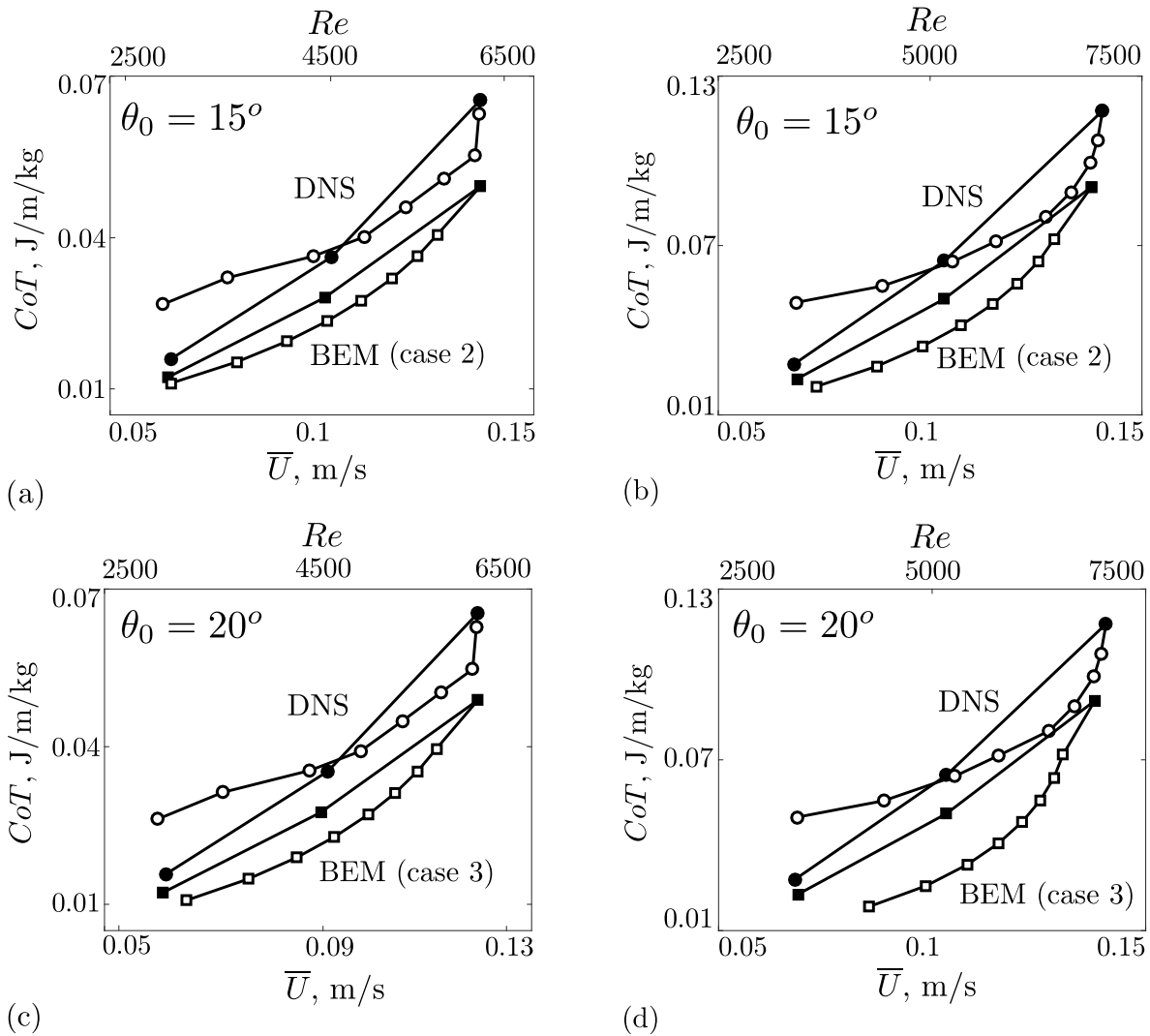
Figure 5: Cost of transport as a function of Re for continuous and intermittent swimmers for (a),(c) $\theta_0 = 15°$ and (b),(d) $\theta_0 = 20°$. The black markers represent continuous gait and white markers represent intermittent gait. Circles and squares are the results acquired in viscous and inviscid flows, respectively. In (a),(c) viscous simulations are compared against the drag case 2 inviscid simulations and in (b),(d) against drag case 3 inviscid simulations.
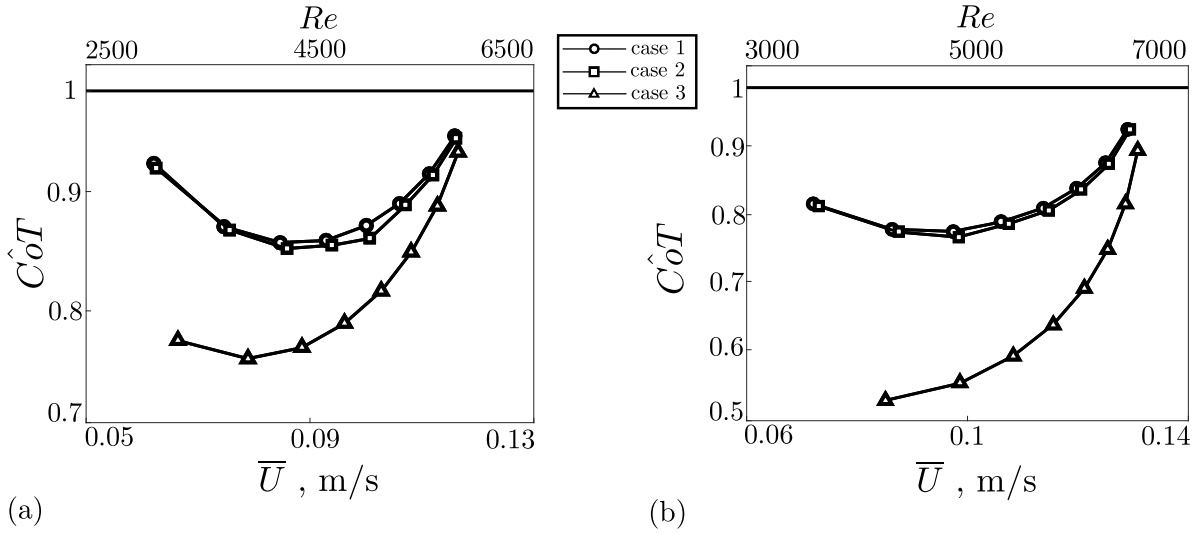
American Institute of Aeronautics and Astronautics

Figure 6: The comparison of dimensionless cost of transport as a function of Re for three set of simulations (a) $\theta_0 = 15°$ and (b) $\theta_0 = 20°$.

is energetically beneficial. If $\hat{CoT} = 1$ then both gaits are energetically equivalent. Finally, if $\hat{CoT} < 1$, then an intermittent gait is energetically beneficial. At the same Re, the cost of transport difference in between the continuous swimmer and the drag law case 1 curve represents the inviscid energy savings out of using intermittent swimming gait. Similarly, the cost of transport difference in between the drag law case 2 curve and the continuous swimming line shows the inviscid benefit plus the benefit coming from the skin friction reduction in the coasting phase. Finally, the difference between the continuous swimmer line and the drag law case 3 curve is the total energy savings coming from the inviscid mechanism and the skin friction/form drag reduction in the coasting phase. A direct observation is, regardless of the pitching amplitude, skin friction attenuation in the coasting period does not play a significant role in energy savings. Skin friction difference in between bursting and coasting periods increases with increasing Re. On the other hand, high Re requires high duty cycle swimming which reduces the coasting period and effect of skin friction attenuation. Therefore, there is a range of medium duty cycles where the trade off in between coasting duration and skin friction change leads to the maximum energy savings out of skin friction attenuation. The larger portion of the savings is coming from the inviscid mechanism. Additionally, drag law case 3 represents that in the limit of very high Re flow, roughly half of the benefit is linked to the form drag attenuation in coasting period and the other half is coming from the inviscid mechanism.

IV. Conclusion

The performance and wake structures of self-propelled intermittently swimming hydrofoils are examined in inviscid and viscous flows. The main vorticity groups observed during the bursting phase of motion are similar in both viscous and inviscid simulations. A total of four vorticity groups are shed from the trailing edge per bursting period. Two vorticity groups are shed as starting and stopping vortices while the other two are shed near the extremes of the pitching motion. The major difference between viscous and inviscid simulations is the formation and shedding of leading-edge vortices during both the bursting and coasting phases leading to additional form drag in a viscous flow.

DNS skin friction and form drag data are also directly used in the BEM simulations to disentangle the relative contributions from the viscous and inviscid energy saving mechanisms. Particularly, three cases of drag laws are applied to the BEM simulations. The first case only investigates the energy savings by the inviscid mechanism alone, that is, the energy savings due to the alteration of the ratio of added-mass thrust-producing to circulatory drag-inducing forces. The second case probes the energy savings from both the skin friction rise and the inviscid mechanism, which is comparable to the low Re DNS data. The third case examines the energy savings estimated in the high Re limit where there is both a skin friction and form drag rise as well as the inviscid mechanism. The energy savings of intermittent swimming at the low Re

(case 2) ranges from 14–24% for $\theta_0 = 15°$–$20°$. At high Re (case 3) the energy savings is estimated to range from 23–44% for $\theta_0 = 15°$–$20°$. The recently discovered inviscid Garrick mechanism is shown to contribute to nearly all of the energy savings observed at low Re ($\mathcal{O}(10^3)$) intermittent swimming while it is estimated that at high Re the inviscid mechanism contributes to half of the energy savings while the other half of the energy savings comes from the Bone-Lighthill viscous mechanism.

V.   Acknowledgements

References

[1] Sfakiotakis, M., Lane, D. M., and Davies, J. B. C., "Review of Fish Swimming Modes for Aquatic Locomotion," Vol. 24, No. 2, 1999, pp. 237–252.

[2] Videler, J. J. and Weihs, D., *Energetic Advantages of Burst-and-Coast Swimming of Fish At High Speeds*, No. 97, 1982.

[3] Videler, J. J., "Swimming Movements, Body Structure and Propulsion in Cod Gadus morhua," *Symp. zool. Soc. Lond.*, 1981, pp. 1–27.

[4] Müller, U. K., Stamhuis, E. J., and Videler, J. J., "Hydrodynamics of unsteady fish swimming and the effects of body size: comparing the flow fields of fish larvae and adults." *The Journal of experimental biology*, Vol. 203, 2000, pp. 193–206.

[5] Lighthill, M. J., "Large-Amplitude Elongated-Body Theory of Fish Locomotion," *Proceedings of the Royal Society B: Biological Sciences*, Vol. 179, 1971, pp. 125–138.

[6] Weihs, D., "Energetic advantages of burst swimming of fish," *Journal of Theoretical Biology*, Vol. 48, 1974, pp. 215–229.

[7] Chung, M.-H., "On burst-and-coast swimming performance in fish-like locomotion," *Bioinspiration & Biomimetics*, Vol. 4, 2009, pp. 036001.

[8] Ehrenstein, U. and Eloy, C., "Skin friction on a moving wall and its implications for swimming animals," *Journal of Fluid Mechanics*, Vol. 718, 2013, pp. 321–346.

[9] Ehrenstein, U., Marquillie, M., and Eloy, C., "Skin friction on a flapping plate in uniform flow." *Philosophical transactions. Series A, Mathematical, physical, and engineering sciences*, Vol. 372, 2014.

[10] Anderson, E. J., McGillis, W. R., and Grosenbaugh, M. A., "The boundary layer of swimming fish." *The Journal of experimental biology*, Vol. 204, 2001, pp. 81–102.

[11] Yanase, K. and Saarenrinne, P., "Unsteady turbulent boundary layers in swimming rainbow trout," 2015, pp. 1373–1385.

[12] Yanase, K. and Saarenrinne, P., "Boundary layer control by a fish : Unsteady laminar boundary layers of rainbow trout swimming in turbulent flows," 2016, pp. 1853–1863.

[13] Akoz, E. and Moored, K. W., "Unsteady Propulsion by an Intermittent Swimming Gait," , No. Lighthill 1971, 2017.

[14] Weihs, D., "Energetic significance of changes in swimming modes during growth of larval anchovy Engraulis mordax," *Fishery Bulletin*, Vol. 77, 1980, pp. 597–604.

[15] Wu, G., Yang, Y., and Zeng, L., "Kinematics, hydrodynamics and energetic advantages of burst-and-coast swimming of koi carps (Cyprinus carpio koi)." *The Journal of experimental biology*, Vol. 210, 2007, pp. 2181–2191.

[16] Katz, J. and Plotkin, A., *Low Speed Aerodynamics*, McGraw-Hill, Inc, 2001.

[17] Quinn, D. B., Moored, K. W., Dewey, P. A., and Smits, A. J., "Unsteady propulsion near a solid boundary," *Journal of Fluid Mechanics*, 2014, pp. 152–170.

[18] Krasny, R., "A study of singularity formation in a vortex sheet by the point-vortex approximation," *Journal of Fluid Mechanics*, Vol. 167, 1986, pp. 65.

[19] Mittal, R., Dong, H., Bozkurttas, M., and Najjar, F. M., "A versatile sharp interface immersed boundary method for incompressible flows with complex boundaries," Vol. 227, 2008, pp. 4825–4852.

[20] Engineering, A., Simulation, C. F., and Rockets, A., *Wake topology and hydrodynamic performance of low-aspect-ratio flapping foils*, Vol. 566, 2006.

[21] Liu, G., Ren, Y., Zhu, J., Bart-smith, H., and Dong, H., "Thrust producing mechanisms in ray-inspired underwater vehicle propulsion," *Theoretical and Applied Mechanics Letters*, Vol. 5, No. 1, 2015, pp. 54–57.

[22] Mechanics, F., "Vortex dynamics and new lift enhancement mechanism of wing body interaction in insect forward flight mechanism of wing body interaction in insect," , No. April, 2016.

[23] Li, C., Dong, H., and Liu, G., "Effects of a dynamic trailing-edge flap on the aerodynamic performance and flow structures in hovering flight," *Journal of Fluids and Structures*, Vol. 58, No. October, 2015, pp. 49–65.

[24] Li, C. and Dong, H., "Three-dimensional wake topology and propulsive performance of low-aspect- ratio pitching-rolling plates," , No. July, 2016.

[25] Wan, H., Dong, H., and Gai, K., "Computational investigation of cicada aerodynamics in forward flight," 2015.

[26] Webb, P. W., Kostecki, P. T., and Stevens, E. D., "The effect of size and swimming speed on locomotor kinematics of rainbow trout," *Journal of Experimental Biology*, Vol. 109, 1984, pp. 77–95.